Article
Numerical Stabilization for Flutter Analysis Procedure

Weixing Yuan * and Xiaoyang Zhang

National Research Council Canada, Ottawa, ON K1A 0R6, Canada
* Correspondence: weixing.yuan@nrc-cnrc.gc.ca; Tel.: +1-613-991-3280

Abstract: Severe mode switching is often observed when the PK-method is used in the flutter analysis of complex aircraft configurations, in particular when nearly 100 vibrational modes are considered. In the commonly used commercial software NASTRAN, the resulting eigenroots are sorted in an ascending order of frequency. Therefore, the appearance of massive mode-switching instances cannot be avoided in the PK-method flutter analyses, especially for engineering applications with real-world complex configurations. In this study, as a post-processing procedure, an extensive sorting capability was developed in order to compensate for NASTRAN's lack of a mode-tracking procedure in between the airspeed steps. The capability was developed based on both the complex eigenvalues and their corresponding eigenvectors. In addition, numerical techniques commonly used in computational fluid dynamics (CFD) were introduced to improve the convergence of the traditional PK-method. A hybrid approach was applied to the initial guess of the reduced frequency, followed by a deferred correction scheme for the PK-iteration process. Additionally, mode matching was specifically addressed when locking eigenroots onto the aerodynamics within the PK iterations. In addition to the PK iterations, a damping iteration or modified *g*-method was implemented by extending the PK-method solver. The combination of these special techniques effectively improved the numerical stability of the iterations in the stability eigensolution process and significantly reduced the appearance of the misleading mode switching, minimizing risks in aircraft flight.

Keywords: aeroelasticity; flutter analysis; PK-method; *g*-method; doublet lattice method; mode tracking; mode matching; aeroelastic eigenvalue

1. Introduction

Aeroelasticity is a multidisciplinary field consisting of aerodynamics, structural mechanics, dynamics, and their interactions. By assuming linear aerodynamics and structural dynamics, classical theories in aeroelasticity are able to predict dynamic aeroelastic instability, i.e., coupled flutter, which may define the stable region of an aircraft flight envelope. These linear theories can be implemented in the frequency or time domains. As they are extremely efficient numerically, frequency domain solutions are generally preferred. However, they contain one important drawback, in particular, in the context of unsteady aerodynamics (Edwards and Wieseman [1]). To consider unsteady aerodynamics effects, the generalized aerodynamic forces (GAF) are formulated in the frequency domain. The GAF, symbolized by $Q(ik)$, are tabulated for a number of sets of discrete reduced frequencies, $k = \omega \bar{c}/2V$, where i is the unit imaginary number, $\bar{c}$ is the characteristic chord length and V is the airspeed. The GAF is not a continuous analytical expression that could be imbedded into the structural force terms to form the full aeroelastic equations, leading to the requirement of an iterative procedure such as frequency matching (Wright and Cooper [2]) because the value of the reduced frequency of k as input to the flutter equation is part of the flutter solution.

Doublet-lattice method (DLM) is the most commonly used method for flutter analysis and certification in industrial practice. DLM is based on the compressible acceleration potential theory for thin wing geometry and it cannot account for the wing thickness nor

capture recompression shocks or boundary layer separations. However, flutter and other aeroelastic problems are often observed in jet aircraft flights, where nonlinear aerodynamic characteristics are present due to local supersonic flow regions terminated by shocks. Since computational fluid dynamics (CFD) becomes mature in capturing shock waves and simulating shock wave–boundary layer interactions, CFD is increasingly used for computational aeroelasticity. In order to achieve this, a number of researchers coupled CFD with computational structural dynamics (CSD) [3–5]. The coupled CFD-CSD approaches effectively showed capability in accounting for the nonlinear aeroelastic effects, including the transonic dip due to compressibility effects and limit cycle oscillations (LCOs). In the fully coupled CFD-CSD methods, the simulations are carried out in the time domain and the structural displacement responds instantly to the forces exerted by the fluid, which requires large computational cost.

As an efficient industrial practice, CFD is also used to correct or replace the DLM in flutter analysis, forming a hybrid linear–nonlinear or time–frequency domain methods. Kaiser et al. applied a CFD-corrected DLM to account for nonlinear effects in a gust-encounter investigation [6]. Fleischer and Breitsamter used CFD methods for the computation of GAFs [7]. A linear frequency domain solver was used for harmonic small-disturbance solutions in [6] while a time-marching Euler method was used to generate the GAFs in [7]. In the latter case, the CFD results obtained in the time domain were transformed to the frequency domain using Fourier analysis for calculation of the GAFs used for the following flutter analysis.

The aforementioned fully coupled CFD-CSD approaches are used in the time domain while the hybrid linear–nonlinear methods use CFD to correct or replace the DLM and its corresponding aeroelastic stability analysis for complex eigensolutions still remains in the frequency domain, the same as in the linear flutter analysis methods. In the widely used linear methods, there are three main steps: 1. Structural modal analysis to generate the real eigenvectors as the vibrational mode shapes; 2. Aerodynamic modelling to generate the aerodynamic influence coefficients (AICs) and GAFs; 3. Aeroelastic stability analysis searching for complex eigensolutions to determine flutter speed. The aforementioned hybrid methods using CFD improve the aerodynamic modelling in Step 2. The present study is focused on numerical stabilizations of the aeroelastic stability analysis process in Step 3.

There exist a number of flutter analysis approaches to solve the frequency-matching problem. Among them, the K-method and the PK-method are most commonly applied. Both methods are based on simple harmonic motion assumptions, which are acceptable at the flutter boundary. However, they are not valid below and above the flutter boundary. Consequently, the methods may predict the same flutter speed and frequency, but with an inaccurate subcritical behavior. It is known that damping predicted using the K-method is not reliable, c.f., Section 5.4.2 in Hodges and Pierce [8]. Therefore, the PK-method is often selected because of its reliability.

The PK-method has wide applications, which are exemplified by the following two recent test cases. Dinulović et al. [9] applied the PK-method to flutter analysis of tapered composite fins based on panel vortex methods. Rho et al. [10] performed a hybrid frequency and time domain analysis to predict aeroelastic phenomena such as flutter, divergence and buffet of a hammerhead launch vehicle, where CFD was employed to calculate the unsteady aerodynamic forces for the vehicle in harmonic vibrating motions in the time domain. The aerodynamic forces were then transferred to the frequency domain for flutter analyses using *v-g* and PK-methods.

In the PK-method, the Mach number, altitude and airspeed are fixed for each iteration, while the reduced frequency is set with an initial guess that is normally a low value. Starting from the mode with the lowest structural frequency, iterations are performed with the reduced frequency of the aerodynamics for each mode until the reduced frequency converges. Then, the iteration process is repeated for the next mode at a higher frequency until a converged solution is obtained for all the structural modes selected by the user.

Since an aeroelastic stability analysis of a real-world complex aircraft configuration may involve up to 100 vibrational modes, severe mode switching is often observed in the flutter analyses when using the commonly applied PK-method of the commercial code NASTRAN. Severe misleading mode switching may cause misidentification of aeroelastic phenomena. As a result, factors leading to instabilities such as flutter and divergence may be improperly interpreted and incorrectly understood, and attempts to make engineering decisions (such as stores clearance by flutter similarity) to improve flight performance could be misguided and likely unsuccessful.

To alleviate the severity of the aforementioned mode switching, mode-tracking methods based on eigenvalues and eigenvectors as a post-processing module have established a more reliable visualization of the mode behavior in flutter analysis. Nevertheless, issues with mode switching have not yet been fully resolved. We believe that mode switching is inherently correlated to the PK iteration process. As pointed out by Eldred et al. [11], the PK-method has a feature where there may be more modes for which the aerodynamics match the complex eigenvalue (root) than the pre-defined structural ones at a given airspeed. The extraneous eigenvalues cause problems for the mode-tracking process since the algorithms may mistakenly lock onto one of these roots if it is similar to the true one.

This is mainly attributed to the fact that in addition to the aeroelastic eigenvalues that emerge from the structural natural frequencies, there can be aerodynamic eigenvalues that emerge from the aerodynamic model itself. Dashcund [12] developed both theoretical and experimental models to study active suppression of flutter of a classical bending–torsion wing by adding a control surface. By comparing the predicted results to the experimental results, it was determined that some aeroelastic roots resulting in divergence were from neither structure nor control system. They were derived from the aerodynamic model instead. By examining the eigenvectors of a two-dimensional (2D) wing that had rigid airfoil sections with permit for rotation only, Heeg [13] reported that the least stable real mode originated in the aerodynamics and became the source of static divergence. This finding was proven by their wind-tunnel experiments using a quasi-2D wing. More recently, Vedeneev [14] confirmed that when applying unsteady aerodynamics to a two-degree-of-freedom (two-DOF) bending–torsion wing, the structural eigenfrequencies became damped while the divergence mode separated from a continuous spectrum that existed in the aeroelastic system due to the wake behind the wing that was embodied in the unsteady aerodynamic model.

There exist a number of mode-tracking techniques. Desmarais and Bennett [15] relied on the shape of the characteristic polynomial for their *v-g* analysis and used Laguerre iteration to converge from a previous to a corresponding current eigenvalue. van Zyl [16] correlated the modes based on complex inner products between current and previous right eigenvectors. Eldred et al. [11] proposed complex higher-order eigenpair perturbations (C-HOEP) and complex cross-orthogonality check (C-CORC) methods. However, they concluded that in their PK-method analysis, van Zyl's method outperformed the C-CORC and C-HOEP methods. Recently, Ren [17] developed a predictor-corrector scheme based on the perturbation theory of eigenvalues for mode tracking and applied it to the piecewise quadratic interpolation (PQI) method proposed by Goodman [18]. The correction scheme adaptively adjusted the speed interval between the current and next speed steps by comparing the estimated eigenvalues and sorted eigenvalues. Similarly, Quero et al. [19] developed a mode tracking algorithm by adapting the interval of the parameter of interest (i.e., airspeed in PK-method) and applied it to the p-L flutter analysis method generalized by Quero et al. [20]. Nevertheless, simply using smaller airspeed intervals in the PK-method did not improve the results for the real-world complex configurations discussed in the present study.

Moreover, solutions with eigenvalues (roots) less than the vibratory mode numbers were also observed in the present study. When the numbers of modes and roots do not match, the post-processing algorithms for mode tracking are no longer effective and can be meaningless. Thus, investigations on the PK iteration process are needed to improve the

numerical stability of the flutter analysis methods instead of pure re-ordering (mode tracking). As expected, this study confirmed that the initial guess and the iteration procedure of the eigensolution are crucial to obtain stable and accurate flutter trends.

It should be noted that a promising *g*-method was proposed by Chen for reliable damping prediction [21]. Gu and Yang further reformulated and solved the damping iterations in a modified PK-method [22]. The methods were well illustrated for wings with less than 10 vibrational modes. However, it has not been confirmed whether the *g*-methods can improve the issues with severe mode switching for real-world complex applications involving dozens of structural modes.

To make use of the structural and aerodynamic data outputted from the commercial finite element software NASTRAN as input to our in-house flutter solver FLUTQ, a communication interface between NASTRAN and FLUTQ was developed in this study. Stabilization techniques were developed and implemented for the PK-method, including mode tracking between airspeeds, mode matching to lock eigenroots onto the aerodynamics, a hybrid scheme for the initial guess of the reduced frequency k, a deferred scheme used for the PK-iteration procedure, and a modified *g*-method using damping iterations. Consequently, the applicability of the in-house solver FLUTQ was extended. As a result, the numerically improved aeroelastic stability analysis effectively minimized the severity of the misleading mode switching often observed in flutter analyses for real-world aircraft. The more reliable prediction and higher clarity of the flutter modes led to less time and effort to understand and interpret the flutter analysis results, with increased confidence that the predictions were valid for reducing risks in flight.

It should be mentioned that one can extract true aeroelastic eigenvalues by allowing the reduced frequency in the unsteady aerodynamic models to be complex. Edwards et al. [23] employed the generalized Theodorsen function for the aerodynamic loading of a 2D thin wing with three-DOF motions. Instead of the assumption of simple harmonic motion, the transient response was solved and the true aeroelastic eigenvalues including the damping ratios and frequencies were obtained. Liska and Dowell [24] applied generalized or complex Theodorsen function in an unsteady aerodynamic model to the aeroelastic equations of a two-segment folding wing. The complex Theodorsen function depends on the motion's frequency and damping, and describes the magnitude and phase of circulatory effects in unsteady aerodynamics. Although exact eigensolutions were obtained in these studies, these methods are computationally expensive. Moreover, the use of analytical aerodynamic models is neither feasible nor realistic for applications to real-world complex configurations.

It should be noted that an initial version of this work was presented in [25]. The major difference between the initial version and this manuscript is that both the eigenvector-based mode tracking technique and a modified g-method were recently implemented in the in-house solver FLUTQ. The FLUTQ results presented in the initial version were neither mode-tracked using the eigenvector-based approach nor obtained with a damping iteration using the modified g-method. In next sections, the numerical methodologies will be briefly described first, followed by demonstrations of the improvement to the results.

2. Overview of FLUTQ Solver

The Aerodynamics Laboratory at the National Research Council (NRC) Canada developed a computer program, FLUTQ, capable of carrying out flutter analyses for subsonic, transonic and supersonic flows in the 1990s and 2000s [26]. This program solves the relevant flutter equation using one of several different methods, including the PK, K, or *v-g* method. The flutter matrix at a particular Mach number, airspeed, altitude and reduced frequency is built up from the structural mass and stiffness matrices (from NASTRAN) and the GAF matrices. The flutter matrix is solved for its complex eigenvalues by reduction to the upper Hessenberg form, which is then solved by the double QR algorithm.

In this study, the NRC in-house flutter solver FLUTQ was extensively debugged and further developed for real-world complex aircraft applications. The development included the following:

1. An interface with NASTRAN was developed. This enabled the FLUTQ solver to communicate with NASTRAN, allowing FLUTQ to perform eigenvalue analyses for flutter predictions using NASTRAN's structural and aerodynamic matrices.

2. The solver was extended to a large number of vibrational modes. The original version of FLUTQ was tested for up to five modes [26], which limited its application to much more complex configurations of aircraft in the real world. During the course of the code development, extensive debugging was conducted.

3. A capability was developed for matched altitude flutter solutions. The original version of the FLUTQ solver was designed for a single pre-defined air density with a single true airspeed. This development introduced air density ratios to allow the density to vary at each equivalent airspeed to match the assumed Mach numbers, enabling matched altitude flutter solutions, same to the procedure that is often used in real-world flutter analyses.

4. NASTRAN PK-method sorts eigenroots in ascending frequencies without a mode-tracking procedure, resulting in unavoidable severe mode switching for complex configuration applications. In the in-house solver, an effective eigenvalue- and eigenvector-based sorting capability was implemented for mode tracking in between airspeed steps, alleviating the appearance of severe mode switching in real-world aircraft flutter analysis results.

5. Mode matching was specially taken care of when locking eigenroots onto aerodynamics within the PK iterations.

6. Inspired by numeric approaches used in CFD, stabilization techniques were further developed and applied to the PK-method for flutter analysis. In particular, a hybrid approach was introduced and applied to the initial guess of the reduced frequency while the PK-iteration process was stabilized by using a deferred correction scheme.

7. Following Gu and Yang [22], a modified *g*-method was implemented in the inhouse FLUTQ solver by extending the PK-method using damping iterations.

All these special techniques effectively improved the numerical stability of the PK iterations in the eigensolution process and appreciably reduced the appearance of mode missing.

3. Methodology Description

3.1. PK-Method for Flutter Analysis

Following Rodden and Johnson [27], the governing equation for aeroelastic stability modal analysis using the PK-method is

$$[M_{hh}p^2 + (B_{hh} - \frac{1}{4}\rho\bar{c}VQ_{hh}^I/k)p + (K_{hh} - \frac{1}{2}\rho V^2 Q_{hh}^R)]\{u_h\} = 0, \qquad (1)$$

where M_{hh}, B_{hh} and K_{hh} are the generalized modal mass, damping and stiffness matrices, respectively. The matrix terms in Equation (1) are all real: Q_{hh}^R and Q_{hh}^I are, respectively, the real and imaginary parts of $Q_{hh}(k, Mach)$ as a function of the reduced frequency k and Mach number. Note that the circular frequency (ω) and the reduced frequency (k) are not independent since $k = \omega\bar{c}/2V$.

The PK-method solution process was described in detail by Bellinger [28]. To improve understanding and aid discussions, the solution process is presented in this work. Equation (1) is rewritten in a canonical form after multiplying by 2,

$$[A - pI]\{\widehat{u}\} = 0, \qquad (2)$$

where $[A]$ is the double-sized real matrix

$$[A] = \begin{bmatrix} 0 & I \\ -M_{hh}^{-1}(K_{hh} - \frac{1}{2}\rho V^2 Q_{hh}^R) & -M_{hh}^{-1}(B_{hh} - \frac{1}{4}\rho\bar{c}VQ_{hh}^I/k) \end{bmatrix}, \quad (3)$$

and $\{\tilde{u}_h\}$ now includes both modal displacements $\{u_h\}$ and their respective velocities $\{\dot{u}_h\}$. In the solution process, the matrix of Equation (2) in canonical form was first reduced to the upper Hessenberg form by using an elimination method, and then the complex conjugate eigenvalues were obtained by using the Double QR-Transformation method. The majority of the eigenvalues of Equation (2) are complex conjugate pairs

$$p = \mathrm{Re}(p) \pm i\mathrm{Im}(p) = \gamma\omega \pm i\omega\sqrt{1-\gamma^2} \approx \gamma\omega \pm i\omega, \quad (4)$$

where ω stands for the modal frequency and γ is the corresponding amplification rate coefficient. Since γ is quite small when near equilibrium or close to flutter points, the imaginary part of the eigenvalue p is simplified to the circular frequency in engineering applications. The reduced frequency k is calculated from the eigenvalue p as

$$k = \frac{\omega\bar{c}}{2V} = \frac{|\mathrm{Im}(p)|\bar{c}}{2V}. \quad (5)$$

Iterations are required for the solution to Equation (2) so that Equation (5) can be satisfied. The iteration is diagrammed in grey in the right plot of Figure 1. It begins with a small non-zero value of reduced frequency k so that Q_{hh}^I/k can be computed. The complex pairs of eigenvalues can be written as

$$p_{rs}^{(j)} = \omega_{rs}^{(j)}(\gamma_{rs}^{(j)} \pm i), \quad (6)$$

where the subscript r stands for the oscillatory mode number that is ordered by frequency ($\omega_{1s} < \omega_{2s} < \ldots$), s is the number of the oscillatory mode under investigation, and j denotes the iteration number of the eigenvalue solution so that the next estimate of the nonzero reduced frequency is

$$k_s^{(j)} = \omega_{s,s}^{(j)}\bar{c}/2V. \quad (7)$$

The iteration is converged when

$$\left| k_s^{(j)} - k_s^{(j-1)} \right| < \varepsilon, \quad (8)$$

where ε stands for the convergence criterion. The converged complex eigenvalues are

$$p_{rs}^{(c)} = \omega_{rs}^{(c)}(\gamma_{rs}^{(c)} \pm i), \quad (9)$$

where only $p_{ss}^{(c)}$ satisfies both Equations (2) and (5), see Bellinger [28]. The search for the next oscillatory mode is started by increasing s by one. Following Rodden and Johnson [27], the first estimate of the next reduced frequency can be

$$k_s^{(0)} = \omega_{s,s-1}^{(c)}\bar{c}/2V, \quad (10)$$

and the iteration process is continued until Equation (8) is again satisfied.

The sequence of calculations for different altitudes or densities, velocities and/or Mach numbers is indicated in the left flow chart in Figure 1. Following Rodden and Johnson [27], the structural damping coefficient required to sustain the simple harmonic motion is calculated as $g = 2\gamma$.
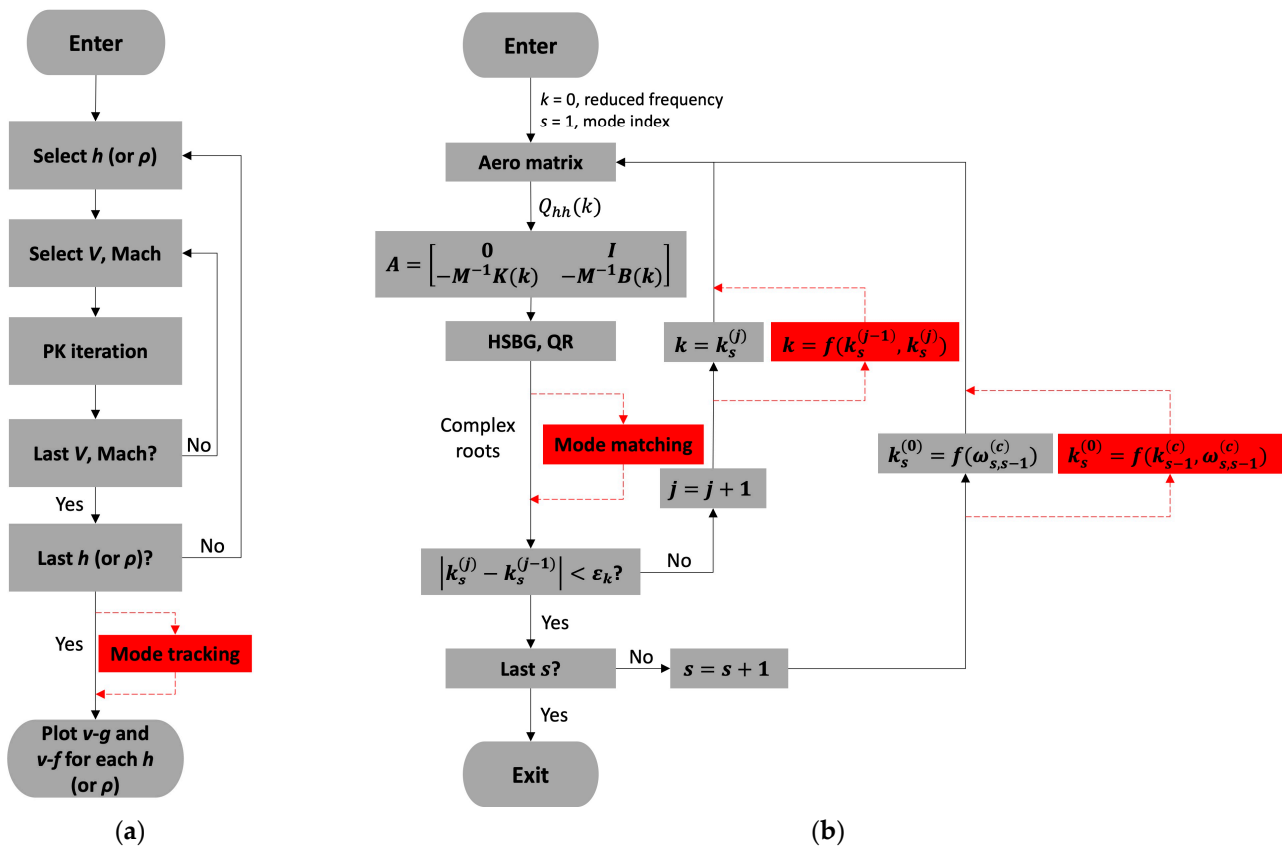
Figure 1. Flow chart of the PK-method, adapted from Bellinger [28]. The right plot (**b**) represents the PK-iteration process in the left plot (**a**). Grey: original processes in NASTRAN; Red: developments in this study.

3.2. Solution Stabilization of the PK-Iteration

Since severe mode switching was observed when using the NASTRAN PK-method for flutter analysis of real-world complex aircraft configurations, numerical technologies were further developed based on NASTRAN. These developments are highlighted in red in Figure 1.

3.2.1. Mode Tracking between Airspeed Steps

In the NASTRAN PK-method, roots are sorted in an ascending order of frequencies. The method does not have a procedure for mode tracking. Two mode-sorting mechanisms were developed and implemented in the in-house flutter solver FLUTQ. Mode sorting was carried out by testing the complex eigenvalues with increasing airspeed. This was a predict-and-select algorithm with following procedures:

1. For each mode, an estimate was made for the complex eigenvalue for the new airspeed using a linear extrapolation based on the two previous airspeeds: $p_{ext} = 2p_{v-1} - p_{v-2}$.
2. The eigenvalue closest to the extrapolated value was selected as the mode for the new airspeed if the new mode was the closest in frequency, i.e., when minimum errors of $|p_{new} - p_{ext}|$ and $|Im(p_{new}) - Im(p_{ext})|$ were determined.
3. The remaining roots were further matched by evaluating whether one of them was within a tolerance band (e.g., δ = 2.5%) of both the real and imaginary parts of the extrapolated eigenroot: $Re(p_{new})$ within $(1 \pm \delta)Re(p_{ext})$ and $Im(p_{new})$ within $(1 \pm \delta)Im(p_{ext})$. This step may be repeated several times by successively increasing the tolerance band.
4. The remaining roots were further matched by evaluating whether one of them was within a tolerance band of the modulus of the extrapolated eigenroot: $|p_{new}|$ within

$(1 \pm \delta) |p_{ext}|$. This step may be repeated several times by successively increasing the tolerance band.

5. Otherwise, one root was selected for the mode under investigation from the remaining eigenroots in an order of increasing modulus.

Figure 2 illustrates the predict-and-select mode tracking procedure. This procedure was imbedded in the FLUTQ solver. Different approaches may be applied to vary the tolerance band δ. Figure 2 exemplifies one of them.
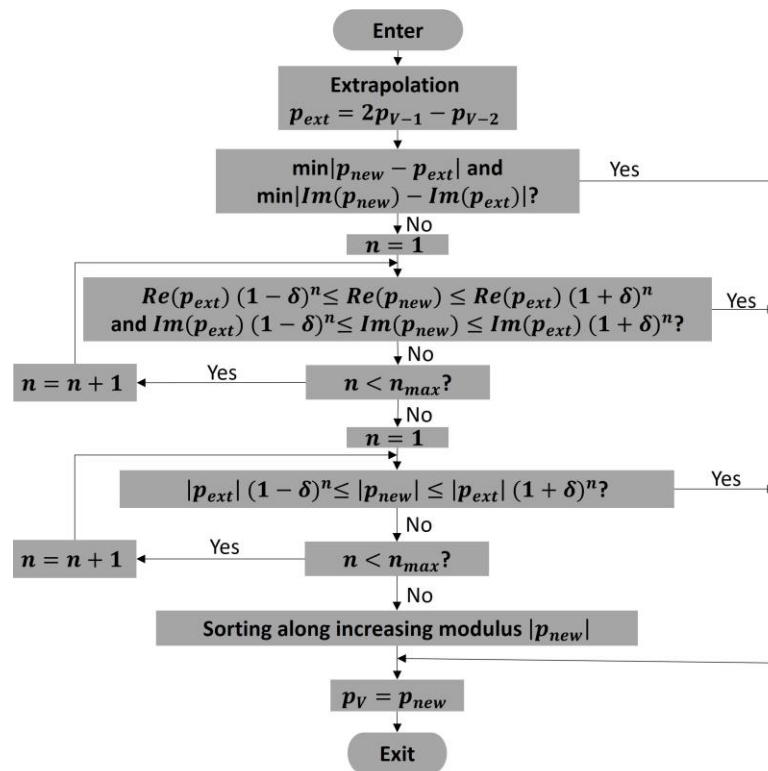

Figure 2. Flow chart of the predict-and-select mode tracking procedure.

In addition, the van Zyl method [16] was employed as a post-processing procedure to the in-house solver. It correlated the modes by using a scalar product of two complex eigenvectors. In simplified terms, it verified if the mode shape was preserved as the airspeed was increased. The procedure is explained here for the solution of the sth mode, at airspeed V_i with increment $i = \{1, \dots, N\}$.

The eigenvalues and eigenvectors pertaining to each mode and airspeed were outputted from the NASTRAN PK-method flutter analyses. As the (right) eigenvectors of the modes $\{Z_R^i\}_s$ were determined, the elements of the correlation matrix were calculated as the scalar product of the complex eigenvectors from the previous and current airspeed steps:

$$C_{sr} = \left\{Z_R^{i-1}\right\}_s \cdot \left\{Z_R^i\right\}_r. \tag{11}$$

The element C_{sr} in row s and column r of the correlation matrix is the scalar product of the eigenvector of the previous airspeed step s and that of the new airspeed step r.

After the correlation matrix was calculated, the largest element of the matrix was determined from a search. The corresponding eigenvectors were taken to correlate to the same mode from the previous to the new airspeed step. The corresponding row and column were then zeroed, the largest element search process was repeated, and another correlation was performed. This process was repeated until the whole correlation matrix was zero and the correlating indexes for all the modes at the ith airspeed were obtained for the new step.

Based on the correlating indices obtained by searching the correlation matrix, the eigenvalues, eigenvectors, frequencies, and damping were re-correlated from the previous airspeed step to the new one. This process was repeated for all airspeeds.

This van Zyl eigenvector-based mode tracking procedure was applied as a post-processor for NASTRAN solutions [29], and some demonstrative results were presented in an initial publication [25]. To apply this procedure to the FLUTQ results, a module for calculating the complex eigenvectors following Rodden et al. [30] was developed in the in-house solver FLUTQ. The eigenvectors were detected within two iterations by using the inverse power method with shifts. The module determined the eigenvector $\{u\}$ from the complex matrix $[A]$ and the complex eigenvalue λ by solving the equation

$$[A - \lambda I]\{u\} = 0, \tag{12}$$

by setting $\lambda = 0$ and $[A] = [M_{hh}p^2 + (B_{hh} - \frac{1}{4}\rho\bar{c}VQ_{hh}^I/k)p + (K_{hh} - \frac{1}{2}\rho V^2 Q_{hh}^R)]$.

3.2.2. Mode Matching to Lock Eigenroots onto Aerodynamics in the PK Iteration

In the PK-method flutter analysis, the number of eigensolution pairs may be more than the defined number of the vibrational modes [11]. This means that more than one pair of eigensolutions of Equation (9) may satisfy Equation (2). However, only one pair of the complex eigenvalues, say the rth in Equation (9), is the right one for mode s under investigation. It is not trivial to determine the right eigenvalue from the eigensolution. According to Bellinger [28], the oscillatory mode number r in NASTRAN is determined based on increasing frequency ($\omega_{1s} < \omega_{2s} < \ldots$): $r = s$. However, the frequency of a mode can either increase or decrease between the airspeed steps, and thus cannot be sorted according to a purely increasing frequency. In this study, the eigenvalue for the mode under investigation was determined based on the previous mode through a two-step mode matching-and-locking procedure:

1. First, a small margin (e.g., 5%) was applied to the neighbouring modes' frequencies, which were then used as the bounds to determine the frequency of mode s under investigation to match the previous mode.

2. Second, when the minimum error of $\left| p_{rs}^{(j)} - p_{(s-1)(s-1)}^{(c)} \right|$ was determined within the bounds, the frequency of eigenvalue $p_{rs}^{(j)}$ was then locked onto the aerodynamics to be used for the $(j + 1)$-th PK-iteration.

3. Otherwise, the eigenvalue $p_{ss}^{(j)}$ was selected from the remaining eigenroots in an order of increasing frequencies and then locked onto the aerodynamics to be used for the next PK-iteration.

4. In case that the frequency increment to the next mode was too large and the next two modes were close in frequency, an extra calculation was performed using a smaller frequency increment (e.g., reducing by 50%) to avoid possibly missing a mode, in particular, when the modes cross during the PK-iteration procedure.

3.2.3. Initial Guess for the PK Iteration

To start the PK iterations, the initial guess of the reduced frequency must be a certain small value close to zero. In this study, the initial reduced frequency was set to 0.001 to start the iteration for the first mode (lowest structural frequency). Once convergence of the current mode was achieved, an updated initial guess was used for the next mode. In NASTRAN, the initial estimate of the frequency is taken from the converged calculations of the previous mode ($s-1$):

$$k_s^{(0)} = \omega_{s,s-1}^{(c)}\bar{c}/2V. \tag{13}$$

This is straightforward to obtain because the eigenroots are ordered in increasing frequencies in NASTRAN. In the previous version of the FLUTQ solver [26], the converged frequency of the previous mode was used as the initial guess:

$$k_s^{(0)} = k_{s-1}^{(c)} = \omega_{s-1,s-1}^{(c)} \bar{c}/2V. \tag{14}$$

To avoid missing any possible modes, both of the initial estimates mentioned above were combined in the present study, leading to a hybrid scheme:

$$k_s^{(0)} = \omega_{s,s-1}^{(c)} \bar{c}/2V + f_{XK0}(\omega_{s-1,s-1}^{(c)} \bar{c}/2V - \omega_{s,s-1}^{(c)} \bar{c}/2V), \tag{15}$$

where f_{XK0} is the weighting factor used for the initial frequency guess. f_{XK0} can be any value between 0 and 1. The NASTRAN format can be recovered with $f_{XK0} = 0$, while the old FLUTQ method can be recovered with $f_{XK0} = 1$. It was determined that $f_{XK0} = 0.6 \sim 0.7$ delivered the most reliable results for the complex aircraft configurations tested in this study. More or less arbitrarily, $f_{RLX} = 0.618$, within this range, was used for the test cases in the present study unless stated otherwise.

3.2.4. Iteration Process of the PK-Method

In NASTRAN, the frequency used for the aerodynamic modeling of the next iteration is simply taken as

$$k_s^{(j)} = \omega_{s,s}^{(j)} \bar{c}/2V. \tag{16}$$

To stabilize the PK-iteration procedure, the deferred correction scheme that is commonly used in the CFD community [31–34] was introduced for the PK iterations, where an under-relaxation parameter, f_{RLX}, was applied to the frequency estimate of the next iteration:

$$k_s^{(j)} = k_s^{(j-1)} + f_{RLX}(\omega_{s,s}^{(j)} \bar{c}/2V - k_s^{(j-1)}). \tag{17}$$

The weighting factor $0 < f_{RLX} \leq 1$, but it is recommended to be in the range of 0.5–0.8. $f_{RLX} = 0.618$ was arbitrarily chosen and used for the test cases in the present study unless stated otherwise.

3.3. Damping Iteration Added to the PK-Method—A Modified g-Method
3.3.1. Formulation of the g-Method

The governing equation for flutter analysis can be written in a general form according to Hassig [35]:

$$\{M_{hh}p^2 + B_{hh}p + [K_{hh} - \frac{1}{2}\rho V^2 Q(p)]\}\{u_h\} = 0, \tag{18}$$

based on the analytical property of the complex function

$$p = \gamma\omega + i\omega = g + i\omega. \tag{19}$$

Applying the Cauthy–Rieman equations and using the damping perturbation method for small g, Chen [21] expanded $Q(p)$ along the imaginary axis (i.e., $g = 0$):

$$Q(p) = Q(i\omega) + gQ'(i\omega), \text{ for } g << 1 \tag{20}$$

$$[M_{hh}p^2 + B_{hh}p + K_{hh} - \frac{1}{2}\rho V^2 Q'(i\omega)g - \frac{1}{2}\rho V^2 Q(i\omega)]\{u_h\} = 0, \tag{21}$$

where

$$Q(i\omega) = Q^R(\omega) + iQ^I(\omega), \tag{22}$$

$$Q'(i\omega) = Q'^R(\omega) + iQ'^I(\omega). \tag{23}$$

It should be noted that $g = \gamma\omega$ is the real part of the eigenvalue p used by Chen [21] while $g = 2\gamma$ is the structural damping coefficient used in NASTRAN (Rodden and John-

son [27]). To be consistent with the notation used in the community, we use $g = 2\gamma$ for the *v-g* and *v-f* flutter trend plots while using the notation $g = \gamma\omega$ for descriptions of the *g*-method in this study.

By comparing Equation (21) with Equation (18), it is straightforward to recognize that there is an added aerodynamic damping term $-\frac{1}{2}\rho V^2 Q'(i\omega)g$, indicating that Equation (18) is only valid for small ω or $g = 0$, or for linearly varying $Q(i\omega)$. By substituting Equation (19), Equation (21) can be rewritten as

$$[M_{hh}g^2 + \left\{ B_{hh} + 2i\omega M_{hh} - \tfrac{1}{2}\rho V^2 Q'(i\omega) \right\}g + K_{hh} - \omega^2 M + i\omega B_{hh} - \tfrac{1}{2}\rho V^2 Q(i\omega)]\{u_h\} = 0. \tag{24}$$

This is the governing equation of the *g*-method proposed by Chen [21]. A reduced frequency-sweep technique is required to search for Im(g) = 0, starting from $\omega = 0$ and increasing ω by $\Delta\omega$. Alternatively, Chen [21] used a predictor–corrector for eigenvalue tracking, which is faster and more efficient:

$$g(\omega + \Delta\omega) = g(\omega) + \Delta\omega \frac{dg}{d\omega}. \tag{25}$$

3.3.2. Implementation of the *g*-Method

The *g*-method was implemented by modifying the PK-method with a damping iteration that is similar to the methodology proposed by Gu and Yang [22]. Solving for the imaginary unit number *i* in Equation (19) provides

$$i = (p - g)/\omega. \tag{26}$$

Substituting Equation (26) into Equations (22) and (23) yields

$$Q(i\omega) = Q^R(\omega) + iQ^I(\omega) = Q^R(\omega) + Q^I(\omega)(p - g)/\omega, \tag{27}$$

$$Q'(i\omega) = Q'^R(\omega) + iQ'^I(\omega) = Q'^R(\omega) + Q'^I(\omega)(p - g)/\omega. \tag{28}$$

Substituting Equations (27) and (28) into Equation (21) yields a PK-method in terms of *p*:

$$[M_{hh}p^2 + B_{hh}p + K_{hh} - \tfrac{1}{2}\rho V^2 \{Q'^R(\omega) + Q'^I(\omega)(p - g)/\omega\}g - \tfrac{1}{2}\rho V^2 \{Q^R(\omega) + Q^I(\omega)(p - g)/\omega\}]\{u_h\} = 0, \tag{29}$$

or

$$[M_{hh}p^2 + (B_{hh} - \tfrac{1}{2}\rho V^2 \{Q^I(\omega)/\omega + Q'^I(\omega)g/\omega\}p + K_{hh} - \tfrac{1}{2}\rho V^2 \{Q^R(\omega) - Q^I(\omega)g/\omega + Q'^R(\omega)g - Q'^I(\omega)g^2/\omega\}]\{u_h\} = 0. \tag{30}$$

Because

$$\omega = k \cdot 2V/\bar{c}, \tag{31}$$

Equation (30) can be further formatted as

$$[M_{hh}p^2 + (B_{hh} - \tfrac{1}{4k}\rho\bar{c}V\{Q^I(\omega) + Q'^I(\omega)g\})p + K_{hh} - \tfrac{1}{2}\rho V^2 \{Q^R(\omega) + Q'^R(\omega)g\} + \tfrac{1}{4k}\rho\bar{c}V\{Q^I(\omega)g + Q'^I(\omega)g^2\}]\{u_h\} = 0. \tag{32}$$

This leads to a modified PK-method with extra aerodynamic terms, as highlighted with red color in Equation (32). When $g = 0$, the added aerodynamic damping terms will disappear and Equation (18) of the PK-method is recovered from Equation (32); thus, the g-method is reduced to the PK-method, or, in other words, the PK-method is a special case of the *g*-method.

The PK-method implemented in the NRC in-house flutter solver FLUTQ was adapted to include a damping iteration $g^{s+1} = \text{Re}(p^{s+1})$ in addition to the reduced-frequency iteration $\omega^{s+1} = \text{Im}(p^{s+1})$ in the solution algorithm. Figure 3 shows a flow diagram for the *g*-method.
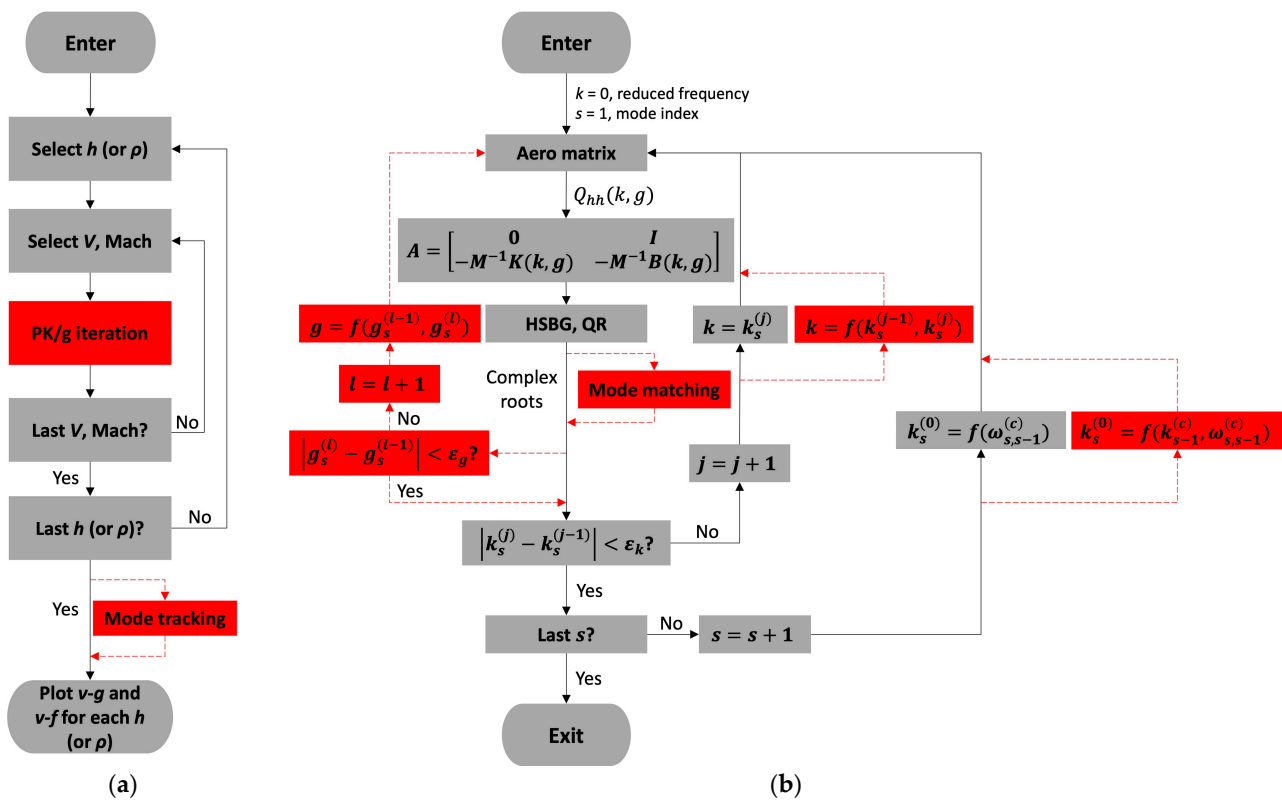
Figure 3. Flow diagram of the modified g-method, adapted from Bellinger [28]. The right flowchart (**b**) represents the damping iteration process added to the left flowchart (**a**). Grey: original processes in NASTRAN; Red: developments in this study.

With the aforementioned extensions, the conventional reduced-frequency "lining-up" process is still performed in the modified algorithm. According to Gu and Yang [22], the modified g-method would provide the same number of roots as the number of structural modes used in the flutter analysis. Note that in the implementation,

$$Q'(\omega) = Q'(k)/(2V/\bar{c}). \tag{33}$$

It should be mentioned that Equation (20) is valid only for $g \ll 1$ [21]. In this study, a bounding with $-0.02 \leq 2\gamma \leq 0.02$ was applied to the calculation of the g damping terms highlighted in Equation (32), unless otherwise stated. Introduction of the bounding limit improved both numerical stabilities and accuracy, which is new when compared with the work by Gu and Yang [22]. This value of the bounding limit was reasonably tested as shown in the results discussion while it coincides with the structural damping commonly considered in the aeroelasticity community. As Wright and Cooper [2] pointed out, some soft or mild flutter may be prevented from occurring due to the existence of structural damping. Thus, the real flutter speed is normally determined from the *v-g* plot by the crossing of an assumed value of structural damping, instead of $g = 2\gamma = 0$. In Wright and Cooper (Sec. 11.5.6) [2] and Edwards and Wieseman [1], the critical damping coefficient was taken as 0.03, while it was assumed as 0.02 for more conservative results in Karpel et al. [36]. Similarly, Gu and Yang [22] assumed a structural damping coefficient of 0.02 in their study.

4. Demonstration and Discussion of the Computed Results

The developed methodologies were first verified against the NASTRAN tutorial example HA145B introduced by Rodden and Johnson [27]. This example presents a flutter analysis of a BAH jet transport wing. The structural, geometric, and aerodynamic parameters are provided by the tutorial in the form of NASTRAN input. Figure 4 shows the BAH wing planform extracted from the NASTRAN user's guide. The aerodynamic

model was divided into six partitions along the semi-span and four boxes chordwise. No motion was assumed at the fuselage centre. Eleven structural grid points are located on the wing, resulting in 10 coupled frequencies of the cantilever wing. The wing properties are reported in detail by Rodden and Johnson [27]. The wing was assumed to be flying in incompressible air (Mach 0.0) and at a dynamic pressure q = 4.0075 psi. The subsonic DLM in NASTRAN was used for the flutter analyses by the PK- or g-methods. The NASTRAN tutorial input files were modified in this study to output the aerodynamic matrix to allow application of the in-house FLUTQ solver.
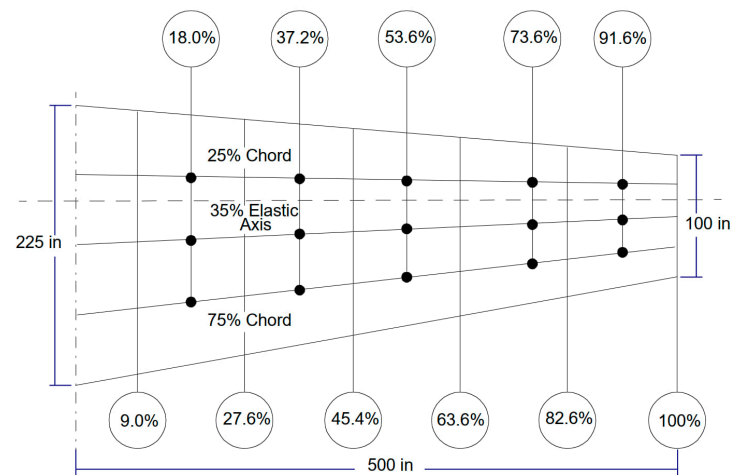
Figure 4. BAH wing planform and aerodynamic boxes (adopted from Rodden and Johnson [27]).

The developed methodologies were applied with the 10 vibrational modes specified. The modal damping and frequency plots obtained with three different techniques are shown in Figure 5, where the top diagrams were from the NASTRAN PK-method, the middle diagrams were from the FLUTQ PK-method, and the bottom diagrams were from the FLUTQ g-method. All three sets of results suggested that a lowest flutter speed is a coupled first-bending first-torsion mode flutter and found in $V_f \approx$ 1054 ft/s and F_f = 3.09 Hz at g(G) = 0. The *v-f* and *v-g* trends were clear with no appearance of mode switching, indicating that all the methods delivered nearly identical flutter results for this simple configuration with only a limited amount of vibrational modes considered. However, the following test cases will exhibit a much more challenging situation for real-world complex aircraft configurations.

After verification using the simple wing model, the improved methodologies were applied to four real-world jet aircraft configurations with underwing and possible tip-mounted stores: two symmetric and two asymmetric configurations as illustrated in Figure 6. The stores represent any objects such as external fuel tanks, weapons, and special electronic sensors or devices. The results were compared with those obtained from NASTRAN.

The flutter analysis model of the real-world jet aircraft was a linear model. A whole-aircraft model was used, which allowed flutter analysis for asymmetric configurations and better prediction of anti-symmetric flutter phenomena. The structural model was a flexible beam or stick model where the fuselage, wing, wing controls and wing tip-mounted stores were modelled by flexible beams and concentrated mass elements. Wing pylons and stores were modelled by a small number of discrete scalar stiffness and concentrated mass elements. The rigid empennage was simply modelled as additional fuselage point masses with no flexibility.
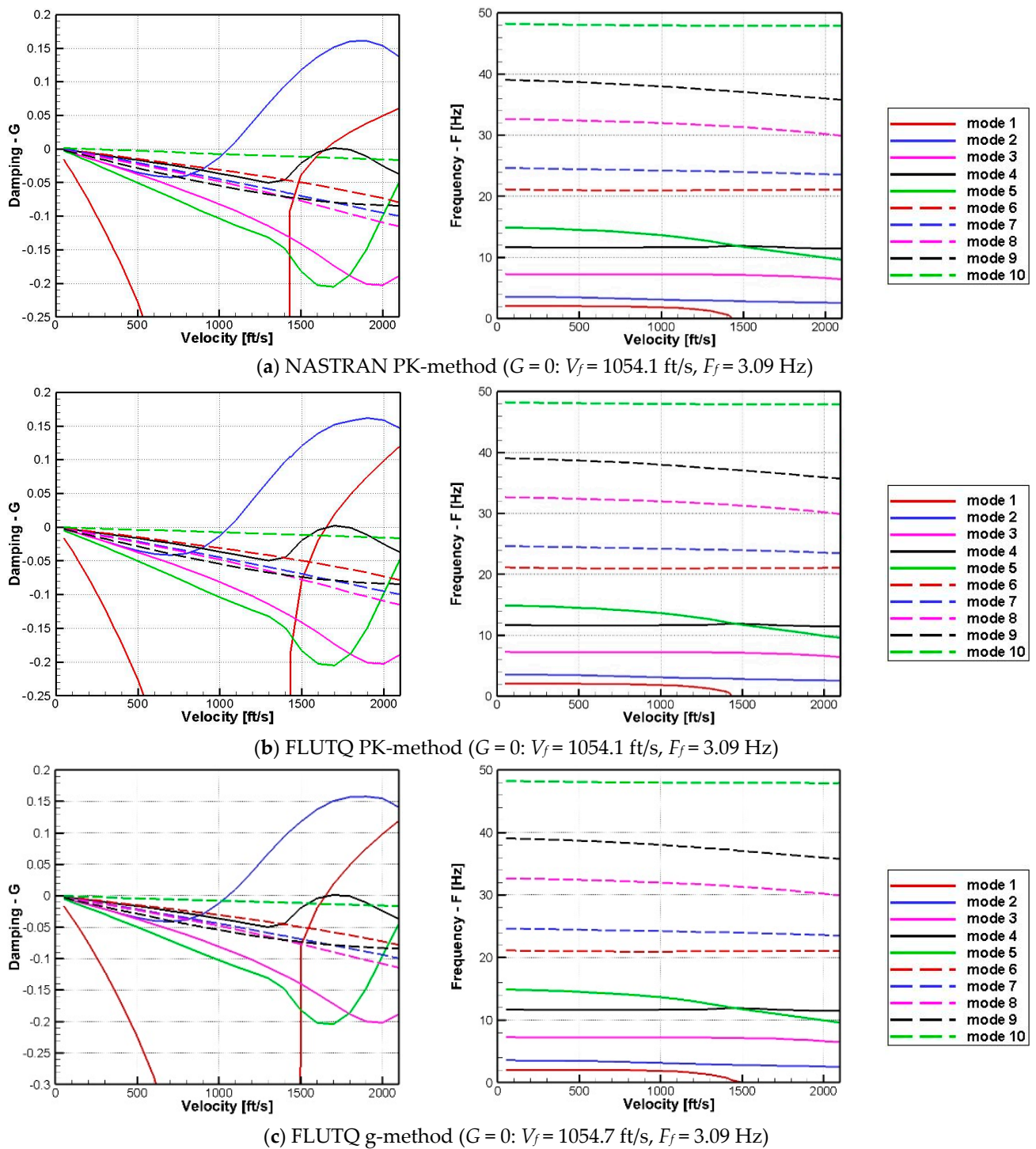
(**a**) NASTRAN PK-method ($G = 0$: $V_f = 1054.1$ ft/s, $F_f = 3.09$ Hz)

(**b**) FLUTQ PK-method ($G = 0$: $V_f = 1054.1$ ft/s, $F_f = 3.09$ Hz)

(**c**) FLUTQ g-method ($G = 0$: $V_f = 1054.7$ ft/s, $F_f = 3.09$ Hz)

**Figure 5.** Damping (**left**) and frequency (**right**) diagrams for the BAH wing.

The aerodynamics of the aircraft were modelled using the DLM. The one-side single wing consisted of 140 panels. The fuselage was modelled by five elliptical-section slender body elements and five cylindrical interference elements. The empennage and underwing stores were not modelled aerodynamically. The tip-mounted store was modelled as an open-ended octagonal cylinder with 184 panels. The flutter analyses assumed the following:

(1)   Mach 0.95 aerodynamics;

(2)   matched altitude flutter solutions, i.e., the air density varied at each speed to match the assumed Mach number;

(3)   80 flutter solution modes for the whole aircraft;
(4)   no structural damping;
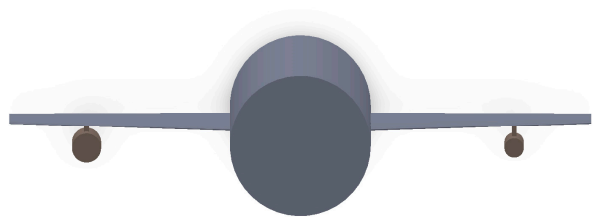(5)   calculation of the $g = 0.0$ flutter crossing.
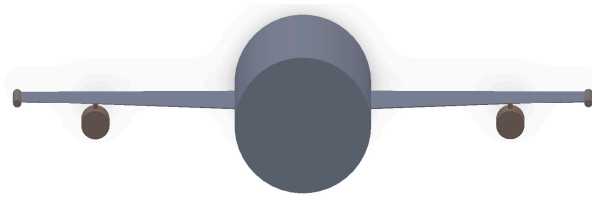
(**a**) Symmetric 1 with tip-mounted stores
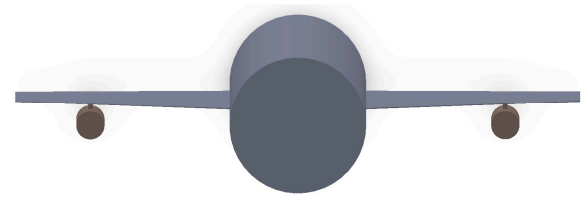
(**b**) Symmetric 2 without tip-mounted stores
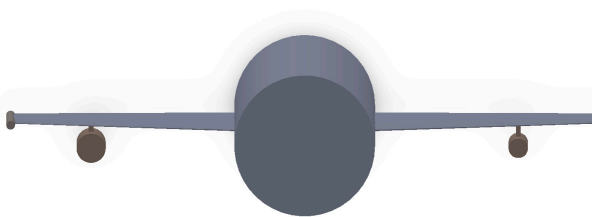
(**c**) Asymmetric 1 with tip-mounted stores

(**d**) Asymmetric 2 without tip-mounted stores

Figure 6. Illustration of the real-world jet aircraft configurations.

The first assumption with Mach 0.95 aerodynamics is obviously rough. As NASTRAN relies on the subsonic DLM, it is not fully possible to determine the unsteady aerodynamic loads to a sufficient accuracy level for transonic conditions. In a study on control surface aerodynamics, Roughen et al. [37] confirmed that DLM results for phase angle agreed well with both CFD and wind tunnel data except for in supersonic regions and cases with high reduced frequency. DLM predicted too small a phase lag in supersonic regions as expected because linear potential theory is not valid in regions where compressibility has a significant influence. Despite the possible inaccuracy, DLM as a common industrial practice has a long history. Triplett used DLM in aerodynamic modelling for F/A-18 wing-store tip-missile flutter at Mach 0.9 and 0.95 [38]. Although the current study is focused on the numerical procedure stabilization in searching for complex eigensolutions, as discussed in the introduction, CFD corrections may improve the accuracy, which should be considered in future studies.

4.1. Effectiveness of the Mode-Tracking Algorithms

Figure 7 shows impacts of the van Zyl [16] method when it was applied as a post-processing mode-tracking procedure to the Symmetric 1 configuration of a real-world complex jet aircraft. The PK-method flutter analysis was conducted using 80 vibrational modes. The first six modes were rigid-body modes. For clarity, the figure displays only the first 14 flexible modes (modes 7–20). The airspeed was arbitrarily normalized in the velocity–damping (*v-g*) and velocity–frequency (*v-f*) plots. The computed damping coefficient G(*g*) indicates the artificial structural damping required to damp the oscillation caused by the interaction between the aerodynamics, structural mechanics, and dynamics. Negative values indicate a stable aeroelastic state while positive values indicate flutter occurrence that requires structural damping to suppress the oscillations. The predicted lowest flutter speeds were $V_f = 77.35\%$ from NASTRAN and $V_f = 77.54\%$ using FLUTQ, with a frequency of 5.69 Hz at $g = 0$. The principal flutter modes were mode 12 (Antisymmetric Wing First Bending) and mode 14 (Antisymmetric Underwing-Store Pitch). As shown in the figure, the mode-tracking algorithm as a post-processing procedure did not change

the flutter prediction results, which was expected. However, it sorted the results and significantly reduced the amount of severe mode switching, thus alleviating confusion in the interpretation of the flutter results. Note that the FLUTQ PK-method results showed less mode switching when compared with the NASTRAN PK-method results.
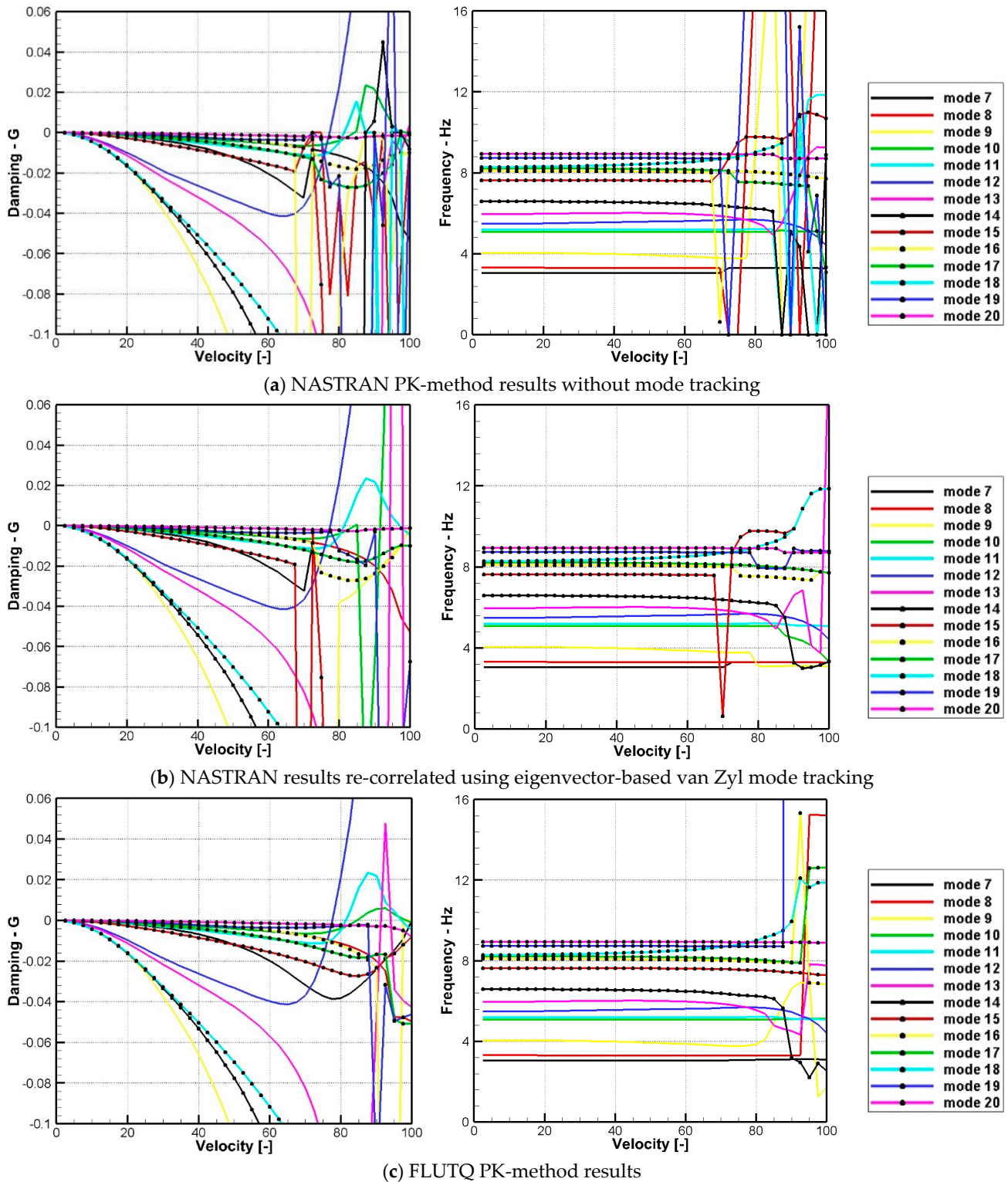

(**a**) NASTRAN PK-method results without mode tracking

(**b**) NASTRAN results re-correlated using eigenvector-based van Zyl mode tracking

(**c**) FLUTQ PK-method results

Figure 7. Effectiveness of mode tracking: damping and frequency diagrams for the Symmetric 1 configuration of the real-world jet aircraft with velocities arbitrarily normalized.

The mode-tracking mechanisms alleviated the severity of the misleading mode switching for some conditions. However, they do not work properly for all complex configurations. Figure 8 demonstrates the ineffectiveness of the eigenvector-based van Zyl mode-tracking algorithm when it was applied to the NASTRAN PK-method results for an asymmetric configuration of the same parent jet aircraft. Although the mode-tracking algorithms reduced mode switching to some extent, the issue related to the mode switching was still obvious. A closer look at the mode-tracking process revealed that the ineffectiveness of the mode-tracking algorithms was mainly attributed to the inaccurate eigensolution. As marked by the red circle in Figure 8b, the solution of a mode was missing in the original eigensolution at airspeed $V = 72.5\%$. The missing solution was inherent to the PK iterations, and the post-processing mode tracking was unable to correct it. As confirmed by Figure 8c, this problem was solved effectively by using the in-house flutter analysis solver. For the Asymmetric 2 configuration, the predicted lowest flutter speeds were $V_f = 61.30\%$ from NASTRAN and $V_f = 61.33\%$ using FLUTQ, with a frequency of 8.08 Hz at $g = 0$. The principal flutter modes were mode 14 (Antisymmetric Fuselage First Bending) and mode 15 (Right Hand Underwing-Store Pitch).
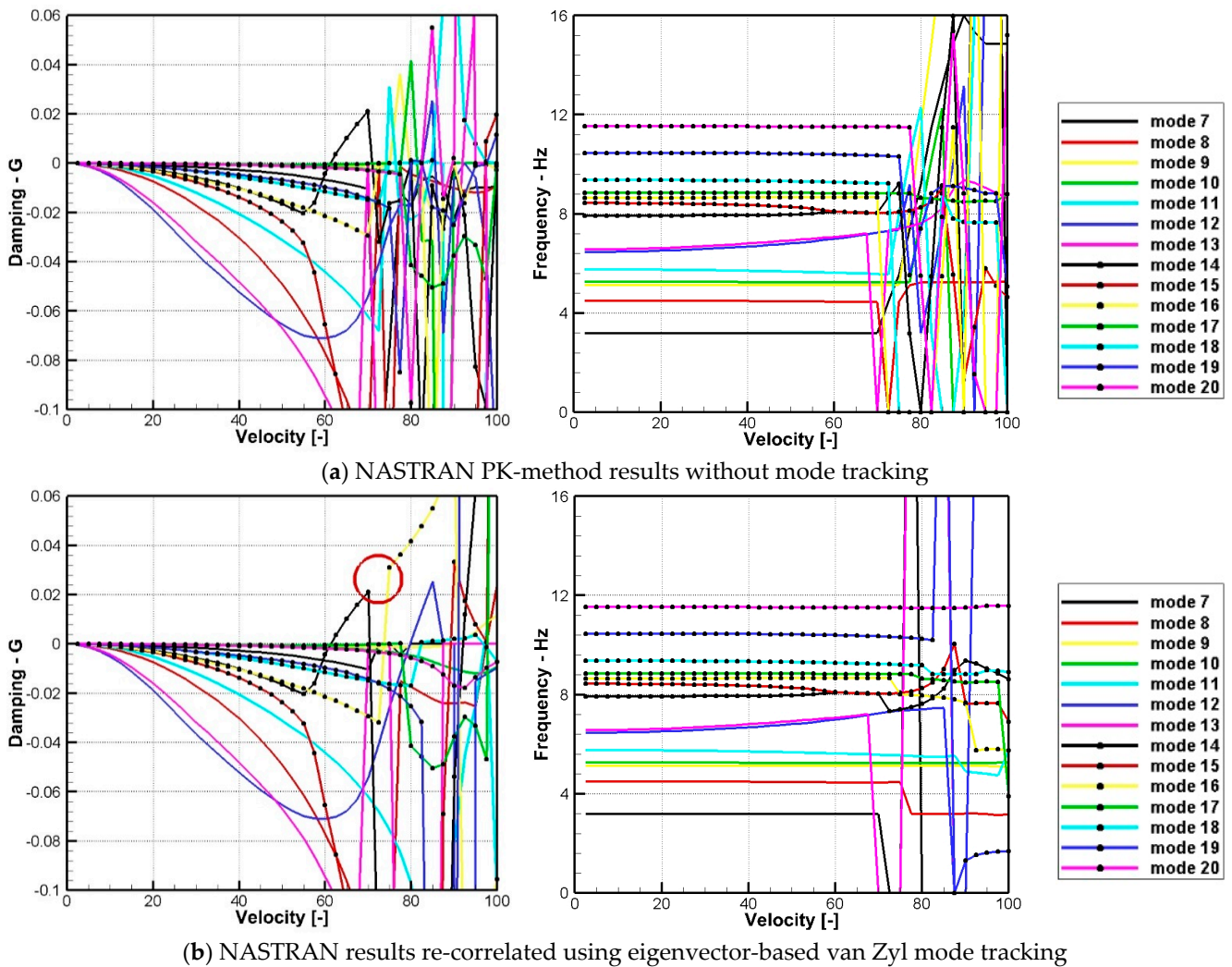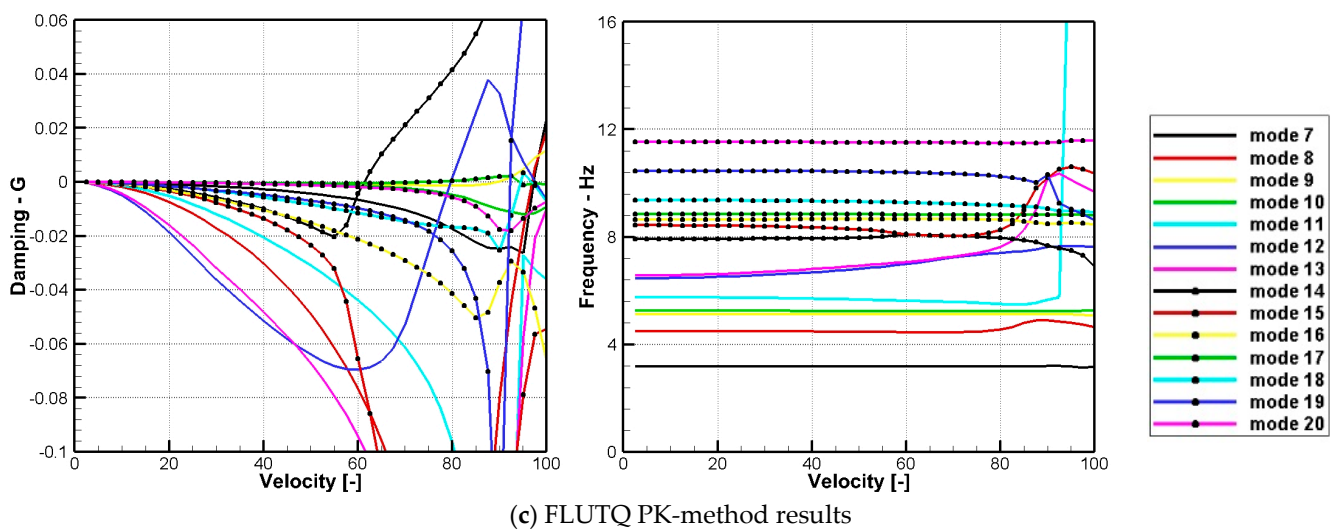

(**a**) NASTRAN PK-method results without mode tracking

(**b**) NASTRAN results re-correlated using eigenvector-based van Zyl mode tracking

Figure 8. *Cont.*

(**c**) FLUTQ PK-method results

Figure 8. Ineffectiveness of mode tracking: damping and frequency diagrams for the Asymmetric 2 configuration of the real-world jet aircraft with velocities arbitrarily normalized.

4.2. Solution Stabilization for the PK-Iteration

Figures 7 and 8 also demonstrate the effectiveness of the solution stabilization applied to the PK-method using the in-house solver FLUTQ. The structural and aerodynamics matrices used for the FLUTQ flutter analyses were the same as those used for the respective NASTRAN solutions. An interface was programed to extract these data from NASTRAN to be employed for the flutter analyses using the FLUTQ PK-method. As shown in the figures, the FLUTQ solutions were extensively improved, and no severe misleading mode switching appeared until the post-flutter region.

Figure 9 further demonstrates the effects of the individual numerical techniques. For simplicity, the figure only displays the first 10 flexible modes. The results shown in Figure 9a demonstrate a test case for which no mode matching-and-locking procedure was used in the PK iterations, confirming that mode matching-and-locking is a key element to stabilize the solution.

The effects of the deferred scheme and the hybrid initial solution on the results were not as obvious as the mode matching-and-locking mechanism. In general, Equations (16) and (13) worked well for most test cases (when other techniques developed in this study were applied). However, introducing the deferred correction scheme in Equation (17) and the hybrid initial solution approach in Equation (14) using under-relaxation parameters alleviated mode switching in the post-flutter region, as evidenced in Figure 10. Mode 15 appeared as a hump flutter mode that crossed $g = 0$ shallowly and then re-crossed to the stable side of the *v-g* plot. Hump flutter modes are most commonly observed in store flutter. The damping of mode 15 was far below 0.02 (an assumed inherent structural damping commonly used in industry) and was believed unlikely to produce explosive flutter. Therefore, the predicted flutter speed was $V_f = 75.54\%$ with a frequency of 7.29 Hz when crossing $g = 0$. The principal flutter modes were mode 12 (Antisymmetric Underwing-Store Pitch) and mode 14 (Antisymmetric Fuselage First Bending). Figure 10a,b show more mode switching, which was mainly attributed to numerical divergences in the post-flutter region when compared to Figure 10c. The under-relaxation parameters provided an additional option to control the numerical stability in the PK iterations.
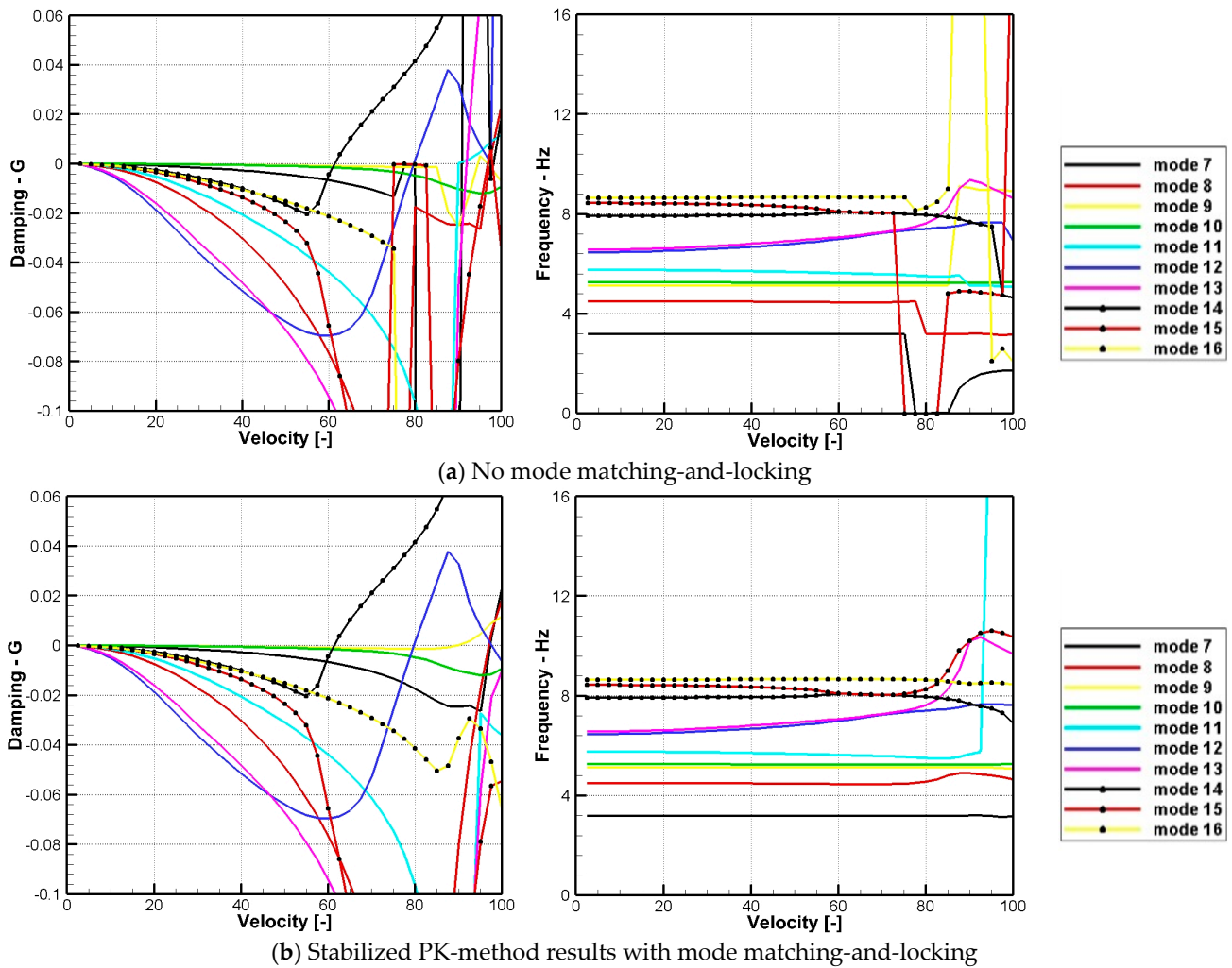
(**a**) No mode matching-and-locking

(**b**) Stabilized PK-method results with mode matching-and-locking

Figure 9. Influence of mode matching-and-locking in the FLUTQ PK-method: damping and frequency diagrams of the Asymmetric 2 configuration of the real-world jet aircraft with velocities arbitrarily normalized.

Note that except for the one under investigation, all other numerical stabilization techniques developed in this study were applied in the demonstration tests of the effects of the individual numerical techniques, which is slightly different from the work presented in our initial publication [25]. Consequently, the results presented in this paper may have a better looking when compared with those presented in the previous paper.

4.3. g-Method Results

The implemented *g*-method was first tested with a NASTRAN tutorial example using the HA145B wing introduced by Rodden and Johnson [27]. After successful verification, the method was applied to flutter analyses of real-world jet aircraft configurations, as performed for the PK-method, to demonstrate its capability.

(**a**) No deferred correction (f_{RLX} = 1) and no hybrid initial solution (f_{XK0} = 1)

(**b**) No deferred correction (f_{RLX} = 1) but with hybrid initial solution (f_{XK0} = 0.618)

(**c**) With deferred correction (f_{RLX} = 0.618) and hybrid initial solution (f_{XK0} = 0.618)
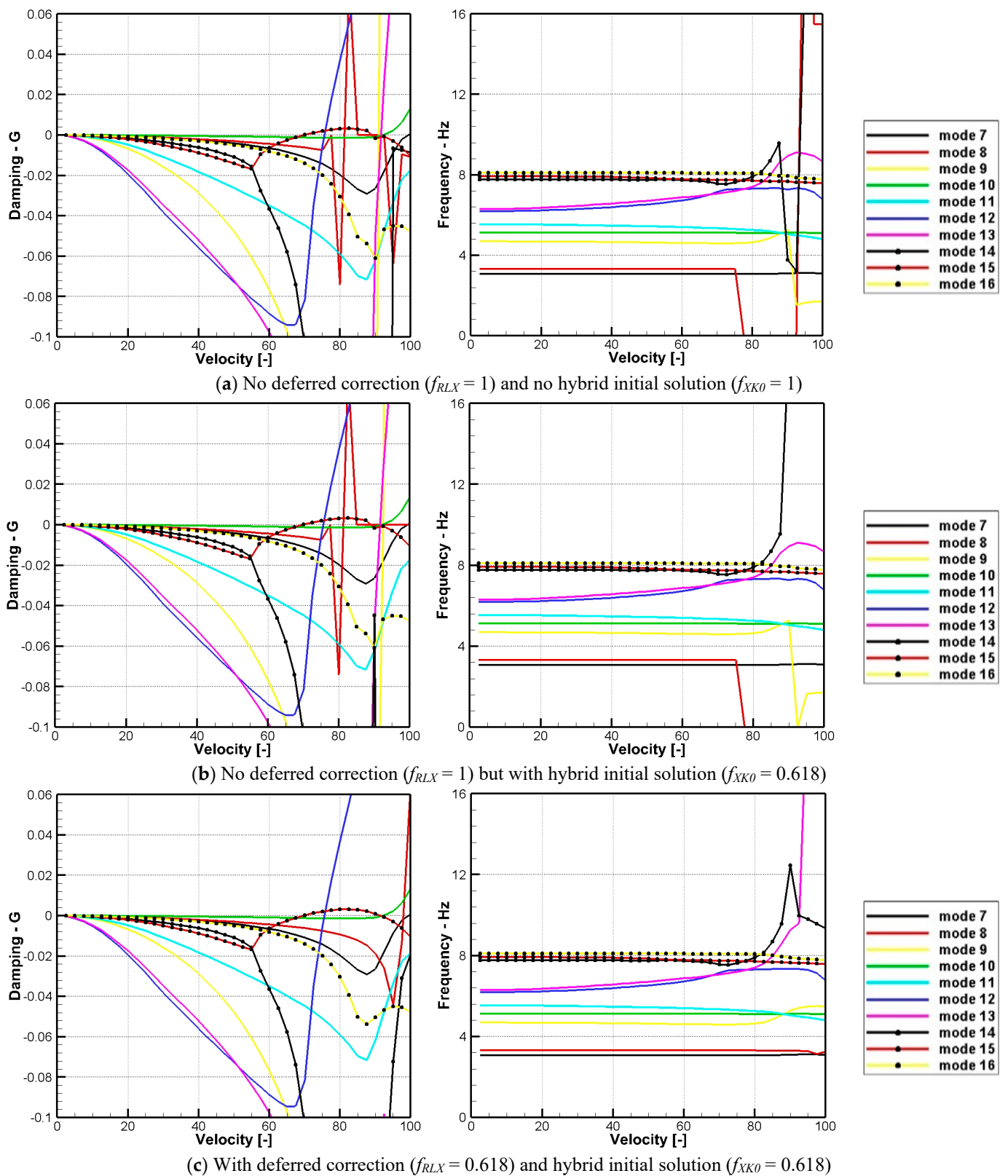
Figure 10. Effects of deferred correction scheme for the FLUTQ PK-method: damping and frequency diagrams of the Symmetric 2 configuration of a real-world jet aircraft with velocities arbitrarily normalized.

Figures 11 and 12 verify the *g*-method implemented in the FLUTQ solver against the PK-method. The predicted flutter speeds for the Symmetric 2 configuration shown in Figure 11 were V_f = 75.53% using the *g*-method vs. V_f = 75.54% using the PK-method, with a frequency of 7.29 Hz when crossing *g* = 0. The principal flutter modes were mode 12 (Antisymmetric Underwing-Store Pitch) and mode 14 (Antisymmetric Fuselage First Bending). The predicted flutter speeds for the Asymmetric 1 shown in Figure 12 were V_f = 82.34% with F_f = 5.70 Hz using the *g*-method vs. V_f = 82.33% with F_f = 5.71 Hz using the PK-method. The principal flutter modes were mode 12 (Left Hand Underwing-Store Pitch) and mode 14 (Antisymmetric Wing First Bending). For the results, both eigenvalue- and eigenvector-based mode-tracking mechanisms were applied to both the PK- and *g*-method results. As shown in the figures, the implemented FLUTQ *g*-method predicted reasonable flutter results. In general, the FLUTQ *g*-method applied to the real-world jet aircraft slightly further reduced the severity of the misleading mode switching in the post-flutter region compared to that of the PK-method. This is because the aerodynamic damping is more realistic when the *g*-method is used.

(**a**) PK-method
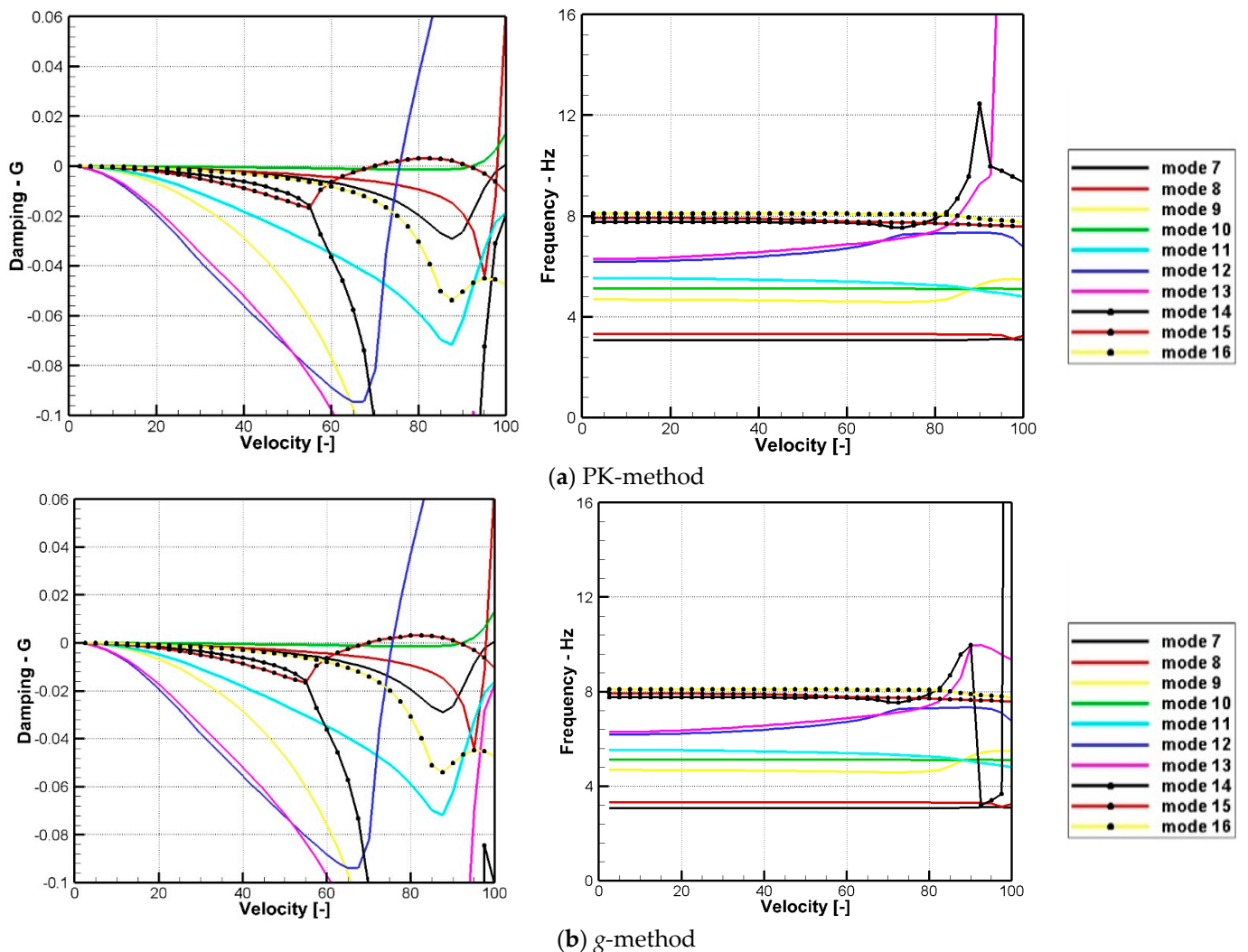
(**b**) *g*-method

Figure 11. Results comparison between the FLUTQ *g*- and PK-methods for the Symmetric 2 configuration of the real-world jet aircraft with velocities arbitrarily normalized.
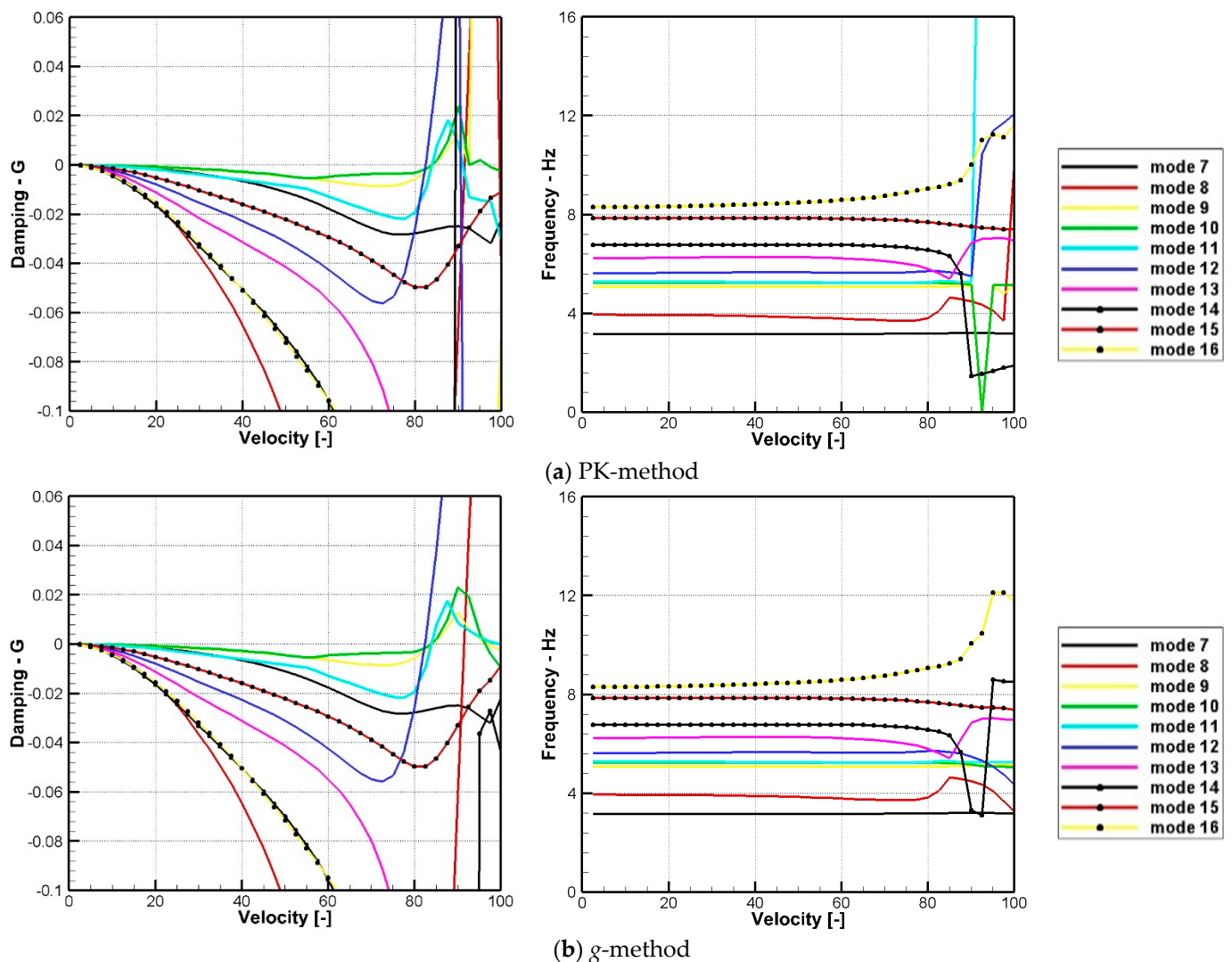
Figure 12. Results comparison between the FLUTQ *g*- and PK-methods for the Asymmetric 1 configuration of a real-world jet aircraft with velocities arbitrarily normalized.

Parametric studies with different numerical settings were also performed for the numerical process in the *g*-method. In general, and as observed in the previous PK-method results, the combined eigenvalue- and eigenvector-based method performed better than either of the individual methods. When using the combined method, the eigenvalue-based mode tracking was performed first, followed by further sorting using the eigenvector-based method in the post-processing.

Slightly different from the PK-method, the deferred correction used for solution stabilization in the *g*-method did not show consistent performance, as observed in the previous PK-method results. In particular, the deferred correction technique improved the results only for some configurations. Therefore, it is recommended to switch off the deferred correction technique when the *g*-method is applied. This will save some computational time because the deferred correction using an under-relaxation parameter may require more iterations for convergence.

As discussed earlier, Equation (20) is valid for $g \ll 1$; therefore, $|2\gamma| \leq 0.02$ was applied to $g = \gamma\omega$ when calculating the damping terms highlighted in Equation (23). To confirm the influence of this parameter, enlarged values of the parameter were studied. In general, $|2\gamma| \leq 0.02$ resulted in the clearest results over the ranges $|2\gamma| \leq 0.04$ and $|2\gamma| \leq 0.1$. Consequently, $|2\gamma| \leq 0.02$ or, in other words, $|g| \leq 0.01\omega$ for Equation (32), is recommended to bound the damping terms in *g*-method flutter analyses for real-

world jet aircraft configurations. Physically, this value used for damping bounding is well aligned with the structural damping coefficient $g = 2\gamma = 0.02$ that is often used to calculate flutter crossing to determine the flutter speed for real-world aircraft configurations when considering realistic structural damping as discussed in Section 3.3.2 when describing the methodologies.

5. Conclusions

In this study, two root-sorting capabilities based on eigenvalues and eigenvectors were developed for the PK-method and implemented in the inhouse solver FLUTQ used for flutter analysis of real-world complex aircraft configurations. Since NASTRAN does not have a mode-tracking procedure, the appearance of severe mode switching instances is unavoidable in flutter results using PK-method for real-world complex engineering applications. The severity of mode switching causes misidentifications and misguidance in the flight envelope development of the aircraft. As a post-processing procedure, mode-tracking technologies help reduce the confusion caused by the mode switching. However, because of the inherent relation with the PK iterations in the eigensolution process, mode tracking may fail in circumstances when the number of eigenroots does not match the number of the vibrational modes.

To improve the flutter analysis, this study focused on the stabilization of the traditional numerical procedure of the PK-method. A hybrid approach for the initial guess of the reduced frequency and a deferred correction scheme for the iteration process were introduced to the numerical procedure for the PK iterations. In addition, a mode-matching-and-locking procedure was introduced when correlating the modes with the aerodynamics. Furthermore, a modified g-method was implemented by adding damping iterations to the PK iteration. The combination of these techniques effectively improved the numerical stability of the eigensolution process and significantly reduced the probability of mode missing.

The proposed techniques were applied to four configurations of a real-world jet aircraft, and the obtained flutter solutions showed significant improvement. Severe mode switching was reduced or eliminated from the subcritical to the post-flutter region when compared against the NASTRAN PK-method results that showed a multitude of instances of mode switching. All the test cases suggested the applicability of the developed techniques to real-world complex engineering configurations. The more reliable prediction and higher clarity of the flutter modes could reduce the time and effort required to understand the flutter analysis results while providing increased confidence that the predictions are valid for decision making to avoid risks of destructive flutter in flight.

the study. It should also be acknowledged that Stuart McIlwain from NRC has provided supportive suggestions in project planning, funding acquisition, and corrections in manuscript writing.

Conflicts of Interest: The authors declare no conflict of interest.

References

1. Edwards, J.W.; Wieseman, C.D. Flutter and Divergence Analysis using the Generalized Aeroelastic Analysis Method. *J. Aircr.* **2008**, *45*, 906–915. [CrossRef]
2. Wright, J.; Cooper, J. *Introduction to Aircraft Aeroelasticity and Loads*; John Wiley & Sons, Ltd.: Chichester, UK, 2007.
3. Yuan, W.; Sandhu, R.; Poirel, D. Fully Coupled Aeroelastic Analyses of Wing Flutter towards Application to Complex Aircraft Configurations. *J. Aerosp. Eng.* **2021**, *34*, 04020117. [CrossRef]
4. Liu, F.; Cai, J.; Zhu, Y.; Tsai, H.M.; Wong, A.S.F. Calculation of Wing Flutter by a Coupled CFD-CSD Method. *AIAA J. Aircr.* **2001**, *38*, 334–342. [CrossRef]
5. Chen, X.; Zha, G.; Yang, M. Numerical Simulation of 3-D Wing Flutter with Fully Coupled Fluid-Structural Interaction. *Comput. Fluids* **2007**, *36*, 856–867. [CrossRef]
6. Kaiser, C.; Friedewald, D.; Nitzsche, J. Comparison of Nonlinear CFD with Time-linearized CFD and CFD-corrected DLM for Gust Encounter Simulations. In Proceedings of the International Forum on Aeroelasticity and Structural Dynamics, Como, Italy, 25–28 June 2017.
7. Fleischer, D.; Breitsamter, C. CFD based Methods for the Computation of Generalized Aerodynamic Forces. In *New Results in Numerical & Experimental Fluid Mechanics, NNFM 121*; Dillmann, A., Ed.; Springer: Berlin/Heidelberg, Germany, 2013; pp. 331–338.
8. Hodges, D.; Pierce, G. *Introduction to Structural Dynamics and Aeroelasticity*; Cambridge University Press: Cambridge, UK, 2011; Volume 15.
9. Dinulović, M.; Rašuo, B.; Slavković, A.; Zajić, G. Flutter Analysis of Tapered Composite Fins: Analysis and Experiment. *FME Trans.* **2022**, *50*, 576–585. [CrossRef]
10. Rho, H.; Nguyen, P.; Bae, J.; Park, S.; Byun, K. Analysis of the Hammerhead Launch Vehicle using CFD-CDE Coupled Method in the Transonic Region. In Proceedings of the 33rd Congress of the International Council of the Aeronautical Sciences (ICAS), Stockholm, Sweden, 4–9 September 2022.
11. Eldred, M.S.; Venkayya, V.; Anderson, W.J. New Mode Tracking Methods in Aeroelastic Analysis. *AIAA J.* **1995**, *33*, 1292–1299. [CrossRef]
12. Dashcund, D.E. *The Development of a Theoretical and Experimental Model for the Study of Active Suppression of Wing Flutter*; Princeton University: Princeton, NJ, USA, 1981.
13. Heeg, J. *Dynamic Investigation of Static Divergence: Analysis and Testing*; NASA: Hampton, VA, USA, 2000.
14. Vedeneev, V.V. New Mechanism of the Aeroelastic Divergence Onset. *AIAA J.* **2000**, *58*, 2716–2725. [CrossRef]
15. Desmarais, R.N.; Bennett, R.M. An Automated Procedure for Computing Flutter Eigenvalues. *J. Aircr.* **1974**, *11*, 75–80. [CrossRef]
16. van Zyl, L. Use of Eigenvectors in the Solutions of the Flutter Equations. *J. Aircr.* **1993**, *30*, 553–554. [CrossRef]
17. Ren, Z. Flutter Analysis and Mode Tracking of Aircraft Model based on Piecewise Interpolation Method. *J. Vibroengineering* **2014**, *16*, 3576–3585.
18. Goodman, C. Accurate Subcritical Damping Solution of Flutter Equation using Piecewise Aerodynamic Function. *J. Aircr.* **2001**, *38*, 755–763. [CrossRef]
19. Quero, D.; Vuillemin, P.; Poussot-Vassal, C. Improved Mode Tracking for the p-L Flutter Solution Method based on Aeroelastic Derivatives. In Proceedings of the International Forum on Aeroelasticity and Structural Dynamics (IFASD 2022), Madrid, Spain, 13–17 June 2022.
20. Quero, D.; Vuillemin, P.; Poussot-Vassal, C. A generalized Eigenvalue Solution to the Flutter Stability Problem with True Damping: The p-l method. *J. Fluids Struct.* **2021**, *103*, 103266. [CrossRef]
21. Chen, P.C. Damping Perturbation Method for Flutter Solution: The g-Method. *AIAA J.* **2000**, *38*, 1519–1524. [CrossRef]
22. Gu, Y.; Yang, Z. Modified p-k Method for Flutter Solution with Damping Iteration. *AIAA J.* **2012**, *50*, 507–510. [CrossRef]
23. Edwards, J.W.; Ashley, H.; Breakwell, J.V. Unsteady Aerodynamic Modeling for Arbitrary Motions. *AIAA J.* **1979**, *17*, 365–374. [CrossRef]
24. Liska, S.; Dowell, E.H. Continuum Aeroelastic Model for a Folding-wing Configuration. *AIAA J.* **2009**, *47*, 2350–2358. [CrossRef]
25. Yuan, W.; Zhang, X.; Poirel, D. Flutter analysis solution stabilization for the pk-method. In Proceedings of the AIAA Aviation Forum, Virtual Event, 2–6 August 2021. AIAA 2021-2473.
26. Su, J. *AEROFLUT—An Aerodynamic and Flutter Analysis Package for Complex Aircraft Configurations: User Guide*; Aerospace Research Centre, National Research Council Canada: Ottawa, ON, Canada, 2007; *unpublished internal document*.
27. Rodden, W.P.; Johnson, E.H. *MSC NASTRAN Version 68 Aeroelastic Analysis User's Guide*; MSC Software Corporation: Santa Ana, CA, USA, 2004.
28. Bellinger, D. *MSC/NASTRAN Aeroelastic Supplement*; The MacNeal-Schwendler Corporation: Los Angeles, CA, USA, 1980.
29. Rocha da Costa, L.; Poirel, D.; Yuan, W. *Mode Tracking Capability Development Applied to Flutter Analysis*; Technical Report; Aerospace Portfolio, National Research Council Canada: Ottawa, ON, Canada, 2016; LTR-AL-2016-0085.

30. Rodden, W.P.; Harder, R.; Bellinger, E.D. *Aeroelastic Addition to NASTRAN. NASA Contractor Report 3094*; The MacNeal-Schwendler Corporation: Los Angalas, CA, USA, 1979.

31. Khosla, P.K.; Rubin, S.G. A Diagonally Dominant Second-Order Accurate Implicit Scheme. *Comput. Fluids* **1974**, *2*, 207. [CrossRef]

32. Ferziger, J.H.; Peric, M. *Computational Methods for Fluid Dynamics*; Springer: Berlin/Heidelberg, Germany, 1996.

33. Yuan, W.; Schilling, R. Numerical Simulation of the Draft Tube and Tailwater Flow Interaction. *J. Hydraul. Res.* **2002**, *40*, 73–81. [CrossRef]

34. Yuan, W.; Khalid, M. Computation of Unsteady Flows past Aircraft Wings at Low Reynolds Numbers. *Can. Aeronaut. Space J.* **2004**, *50*, 261–271. [CrossRef]

35. Hassig, H. An Approximate True Damping Solution of the Flutter. *J. Aircr.* **1971**, *8*, 885–889. [CrossRef]

36. Karpel, M.; Moulin, B.; Chen, P. Extension of the g-method Flutter Solution to Aeroservoelastic Stability Analysis. *J. Aircr.* **2005**, *42*, 789–792. [CrossRef]

37. Roughen, K.; Baker, M.; Fogarty, T. Computational Fluid Dynamics and Doublet-Lattice Calculation of Unsteady Control Surface Aerodynamics. *J. Guid. Control Dyn.* **2001**, *24*, 160–166. [CrossRef]

38. Triplett, W.E. Wind Tunnel Correlation Study of Aerodynamic Modeling for F/A-18 Wing-Store Tip-Missile Flutter. *J. Aircr.* **1984**, *21*, 329–334. [CrossRef]